Particle Accelerators
1973, Vol. 5, pp. 215–226

SLOW BEAM EXTRACTION FROM THE JINR SYNCHROPHASOTRON

I. B. ISSINSKY, S. V. KALYONOV, E. M. KULAKOVA, S. A. NOVIKOV, B. D. OMEL'CHENKO, N. I. PAVLOV, V. F. SIKOLENKO, B. V. VASILISHIN, V. I. VOLKOV and L. P. ZINOVIEV

Laboratory of High Energies, Joint Institute for Nuclear Research, Dubna, USSR

A slow extraction system designed at the Laboratory of High Energies operates on the $\nu_x = 2/3$ radial betatron resonance and permits extraction of more than 90 per cent of a circulating beam by means of two internal magnets.

The high magnetic field operating region is large enough to permit a gain in amplitude at the septum-magnet entrance of about 17 cm per turn and to avoid influence of the field nonlinearity upon the beam emittance. Resonance conditions are created by means of two pole-face windings. The first of these builds up the second azimuthal harmonic of the sextupolar perturbation and the second one reduces the field index from the operating point ($n = 0.67$) to its resonance value ($n = 0.624$).

The first internal lens placed downstream from the septum magnet focuses the beam in a horizontal plane to create an intermediate image located between the septum and extraction magnets. Under these conditions average values along each particle path in the accelerator fringing field are approximately equal and, consequently, the transverse phase volume distortions are small. As the average beam angle at the septum-magnet entrance changes during the extraction time, the septum-magnet field is modulated accordingly.

The beam bending in the extraction magnet is large enough (about 100 mrad) to steer the beam outside the vacuum chamber and to avoid a significant influence of the fringing field in the next quadrant.

The preliminary calculation of the extraction system was made by the analytical method and then on a computer taking into account the circulating beam characteristics, measured distribution $n(x)$, accelerator structure and contribution of pole-face winding currents. Adjustment and experimental study of the system showed a good agreement with calculated results.

The applications of real time feedback control loops into power supplies of the resonance winding and septum magnet allows us to improve significantly the extraction uniformity and to eliminate a slow drift of the beam entering the extraction magnet. The beam size on the first external target is 4×18 mm^2.

The slow extracted beam efficiency has been determined in the reaction on carbon and by measuring the correlation of integrated particle fluxes around the accelerator proportional to the number of protons lost inside the accelerator chamber with the extracted system on and off. According to this method, the efficiency is 94 ± 0.5 per cent.

1. INTRODUCTION

A synchrophasotron slow beam extraction system is based on the $\nu_x = 2/3$ radial betatron resonance and permits extraction of more than 90 per cent of a circulating beam. A high extraction efficiency is achieved due to a great gain in amplitude at the septum magnet entrance in 3 turns (about 17 cm) because the size of the high magnetic field operating region is large enough and the field nonlinearity influence is removed.[1,2]

The plan view of the equipment of the slow extraction system is shown in Figure 1. The first septum magnet *FM* and radial-focusing septum lens *FL* are placed in the straight section between the quadrants I and II. They form the beam at the entrance of the second stage of the internal transport system located in the next straight section. The operating position of the first septum magnet is fixed at a distance $x_s = 35$ cm from the vacuum chamber centre and therefore it must be rammed The choice of this distance is connected with the beam behaviour under resonance conditions determined by magnetic field nonlinearities. The location of the second internal stage that also consists of a magnet *BM* and lens *BL* is chosen at a distance $x = 70$ cm and allows, (a) to shift the beam by $\Delta x = 37$–40 cm with the help of the first stage; this corresponds to a beam bending angle of about 14 mrad and requires a minimum width of the *FM* septum; (b) to pass a negligible part of the second quadrant fringing field without crossing the region of string nonlinear gradients ($x = 80$–85 cm); (c) to construct the second stage in fixed position (the inflector distance from the vacuum chamber centre is 63 cm): (d) because there are no limitations on the weight of the second stage, it may be long and strong enough (its length is comparable with the straight section length); (e) and, consequently, to bend the particles clear of the synchrophasotron

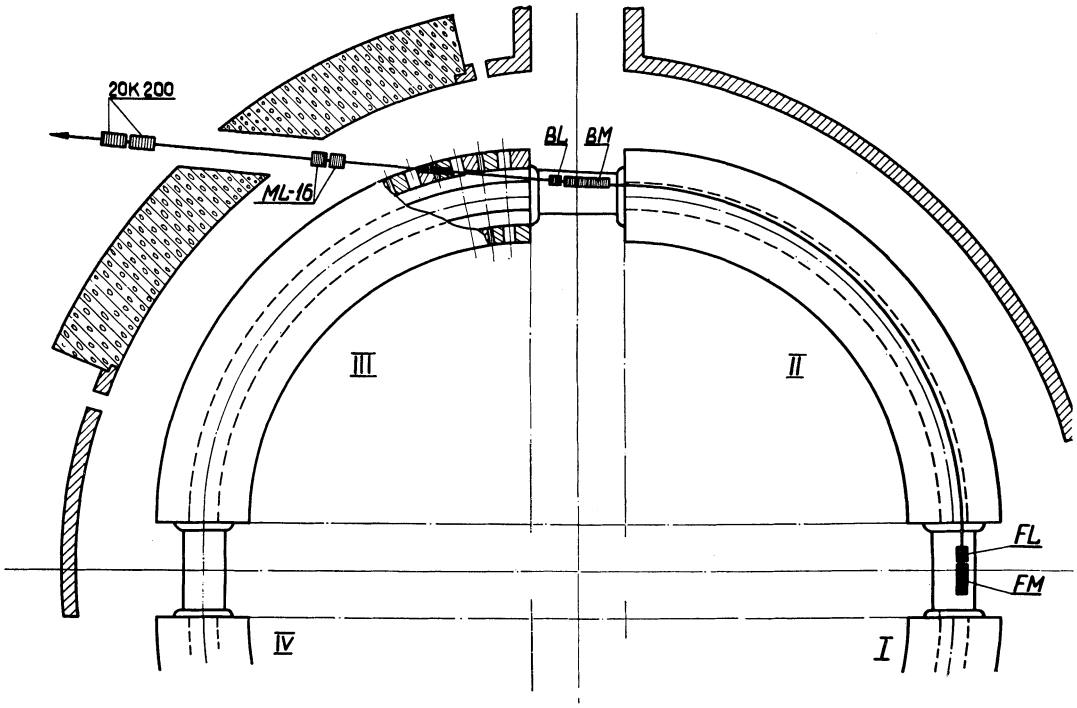

FIGURE 1 Plan view of the equipment of the slow extraction system: *FM*—septum magnet, *FL*—lens, *BM* and *BL*—extraction magnet and lens, *ML*—16 and 20K200—quadrupole lenses of the external transport system, I-IV —accelerator quadrants.

magnet in this way so that they avoid the third quadrant fringing field nonlinearities.

The first stage of the external transport system comprises two quadrupole lens doublets.

The $\nu_x = 2/3$ resonance excitation at the JINR synchrophasotron is created by means of two pole-faced windings. The winding P1 involving 8 pole-face conductors located at the distances $x = \pm 10$ cm and $x = \pm 30$ cm reduces the field index from the operating point ($n = 0.67$) to its resonance value ($n = 0.624$). The pole-face conductors of the winding P2 are located at the distances $x = \pm 20$ cm and $x = \pm 40$ cm and build up the second azimuthal harmonic $\Delta B_z(x,0)$ of the quadratic nonlinearity. As the vacuum chamber construction allows placement of high current pole-face conductors with a distance of 10 cm between them, the quadratic dependence $\Delta B_z(x)$ is formed by means of currents in the winding P2. Both pole-face winding conductors are connected so that the dipole field component at the central accelerator radius is absent (Figure 2).

From different available methods for shrinking of the stable region of weak focusing accelerators[3] we choose the following.

The beam radius is fixed (R_0) and $\Delta B_z(x,\theta)$ is built up. In this case the field index reduces to the resonance value n_r during the accelerator flat top.[3] The advantage of this method is that the extraction efficiency is approximately constant and the resonance control is quite simple. The change of the average beam angle at the *FM* entrance is compensated by a corresponding change in the *FM* current during the beam extraction.

The main relations describing the beam behaviour under these resonance conditions and the preliminary parameters of the extraction system have been calculated analytically. Later, the dynamic beam characteristics and extraction system performance were computed taking into account the measured synchrophasotron parameters.

2. ANALYTICAL ESTIMATE OF THE RESONANCE SYSTEM PARAMETERS

The analysis of particle motion under the $\nu_x = 2/3$

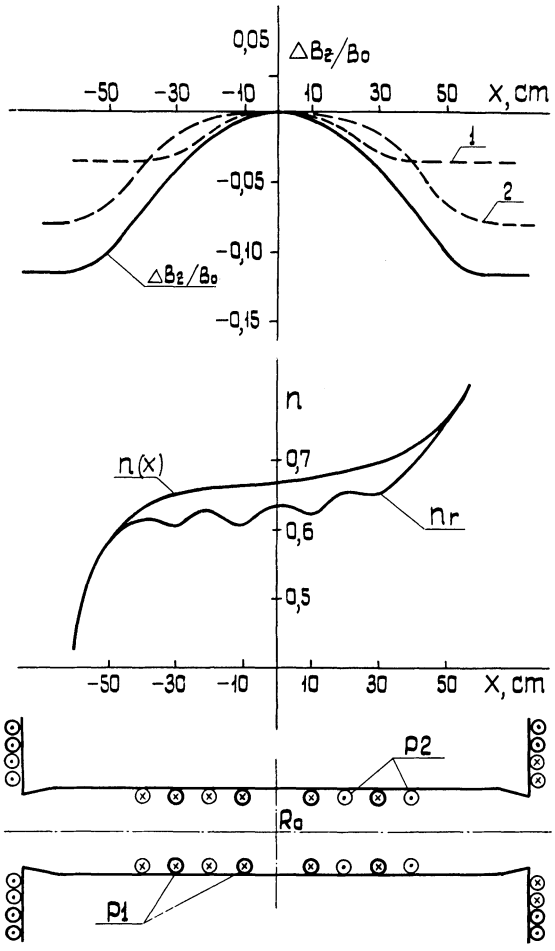

FIGURE 2 Positions of the conductors of the pole-face windings P1 and P2 and additional fields created by them. Curves 1 and 2—field distributions of the single conductors of the winding P2, $\Delta B_z/B_0$—total field distribution, curve $n(x)$—initial field index vs. radius for the synchrophasotron at $B_0 = 10$ kG, curve n_r—field index distribution showing the effect of the winding P1.

resonance conditions was made using a 'smooth' approximation, and the second magnetic field harmonic versus R was presented as:

$$B_z = b_0 + b_1 x + b_2 x^2, \tag{1}$$

where $x = R - R_c = R - R_0 I$ is the particle distance from a 'smooth' equilibrium radius, R_c; R_0 is the central radius in the accelerator quadrants; $I = 1 + 2L/(\pi R_0)$; L is the straight section length. Under these conditions the equation of betatron oscillations at $z = 0$ is:

$$x'' + (1-n)Ix = -(K_0 + K_1 x + K_2 x^2)\sin 2\theta, \tag{2}$$

where θ is the azimuth; $K_m = (4/\pi)(R_c/B_c)b_m (m = 0, 1, 2)$; $B_c = R_0 B_0/R_c$; B_0 is the vertical magnetic field component at the radius R_0.

Influence of the Term K_0

If Eq. (2) takes the form:

$$x = x_1 + \frac{K_0}{4-(1-n)I}\sin 2\theta,$$

$$x' = x' + \frac{2K_0}{4-(1-n)I}\cos 2\theta, \tag{3}$$

then with an accuracy up to the values of the second order K_0, K_1, K_2 the equation for x_1 has been obtained:

$$x'' + \left\{1 - \left[n - \frac{K_0 K_2}{[4-(1-n)I]I}\right]\right\} Ix_1 = -(K_1 x_1 + K_2 x_1^2)\sin 2\theta. \tag{4}$$

Comparison of Eqs. (2) and (4) shows that the presence of the term K_0 in field perturbation leads to the equilibrium orbit distortion[5] described by formula (3) and shifts the effective value of n by

$$\delta n = -\frac{K_0 K_2}{[4-(1-n)I]I}.$$

This fact explains the observed increase of the field index in accelerators under resonance conditions.[3,6]

Later on we consider the equation:

$$x'' + (1-n)Ix = -(K_1 x + K_2 x^2)\sin 2\theta, \tag{5}$$

where x is now the distance from the distorted equilibrium orbit and n is the effective field index.

Equations in Phase Space

Equation (5) was solved using the first approximation of the Krylov–Bogolyubov method.[7] The field index versus radius was presented in the form $n(x) = n_0 + n_1 x + n_2 x^2$. The equations for amplitude and phase at the azimuth $\theta = 0$ were obtained in the rectangular coordinate (x,u) system where

$$u = x'[(1-n)I]^{-1/2}$$

$$\frac{dx}{d\theta} = \frac{3}{16}K_2(x^2-u^2) - \frac{3}{4}I\Delta n u - \frac{9}{16}In_2 u(x^2+u^2),$$
$$\frac{du}{d\theta} = -\frac{3}{8}K_2 xu + \frac{3}{4}I\Delta n x + \frac{9}{16}In_2 x(x^2+u^2). \quad (6)$$

In these equations $\Delta n = n_0 - n_r$. Here n_r is the resonance field index. The absence of the terms n_1 and b_1 indicates that they do not influence the resonance in this approach.

Main Parameters of the Resonance System and Beam Characteristics at the FM Entrance ($n_2 = 0$)

The fixed point coordinates[8] of system (6) are equal to:

$$x_1 = 0, \quad u_1 = 0; \quad x_2 = 0, \quad u_2 = -4I\Delta n/K_2;$$
$$x_{3,4} = \pm 2\sqrt{3}\frac{\Delta nI}{K_2}, \quad u_{3,4} = \frac{2\Delta nI}{K_2}. \quad (7)$$

The first of them is a stable point of the type 'centre' and the others are unstable fixed points defining the size of the stable region. The phase trajectories outside this stable region go to infinity. The stable region reduces to 0 at $\Delta n \to 0$ and does not depend on the Δn sign.

The circulating beam area in phase space ($x x'$) is:

$$S_0 = \pi a_0^2\sqrt{(1-n)I}, \quad (8)$$

where a_0 is the maximum amplitude. By adiabatic changing of n the initial ellipse transforms so that its phase space is constant. The extraction begins when the space phase transforms to a triangle. The area of the triangle is:

$$S = 12\sqrt{3}\left[\frac{\Delta n_b I}{K_2}\right]^2\sqrt{(1-n_b)I}. \quad (9)$$

The condition of the equivalence of the areas (8) and (9) defines the field index difference corresponding to the extraction beginning[1]:

$$\Delta n_b \approx \frac{a_0 K_2\sqrt{\pi}}{2I\sqrt[4]{27}}. \quad (10)$$

As it follows from (6) and (7), if *FM* is placed at $x > 0$ and $\Delta n > 0$, the phase plane points corresponding to the particles at the magnet entrance move approximately along the straight line $u = 2\Delta nI/K_2$, if the change of n is adiabatic. This means that the particle angle at the magnet entrance changes during the extraction from

$$\alpha_b = 2\Delta n_b I\sqrt{(1-n_b)I}/K_2(R_c + x_s) \quad (11)$$

at the extraction beginning to $\alpha_e = 0$ at the end.

If a representative point moves along the straight line $u = 2\Delta nI/K_2$, Eqs. (6) take a more particular form:

$$\frac{dx}{d\theta} = \frac{3}{16}K_2(x^2-x_3^2), \quad \frac{du}{d\theta} = 0. \quad (12)$$

The integration of (12) gives a step per 3 turns at the septum coordinate:

$$\Delta x_s = (x_s^2 - x_3^2)[\exp(-9\pi K_2 x^3/4) - 1]/$$
$$[x_s + x_3 - (x_s - x_3)\exp(-9\pi K_2 x_3/4)].$$

If $9\pi K_2 x_3/4 \ll 1$, the formula takes a more simple form:

$$\Delta x_s \approx \frac{9}{8}\pi K_2(x_s^2 - x_3^2). \quad (13)$$

The maximum value Δx_m corresponds to $\Delta n = 0$ ($x_3 = 0$).

Using (13) and taking into account that the particle density is proportional to $1/\Delta x_s$, we can obtain the expression for the extraction efficiency:

$$E_f = 1 - \int_{x_s}^{x_s+\delta}\frac{8dx}{9\pi K_2(x^2-x_3^2)}\Big/\int_{x_s}^{x_s+9\pi K_2(x_s^2-x_3^2)/8}\frac{8dx}{9\pi K_2(x^2-x_3^2)} \approx 1 - \frac{8\delta}{9\pi K_2(x_s^2-x_3^2)} \quad (14)$$

where δ is the septum thickness.

The results obtained permit some numerical estimates. For $x_s = 35$ cm and $\Delta x_s = 17$ cm, K_2 is equal to 0.0037 cm^{-1}. At the JINR synchrophasotron $n_r = 0.624$. The 'detuning' Δn_b and field index n_b corresponding to the extraction beginning ($a_0 = 8$ cm) are 0.0097 and 0.6337. The mean particle angle at the septum entrance changes from 1.2 mrad up to 0 and the extraction efficiency from 0.965 up to 0.969 for the septum thickness 0.5 cm during the extraction time.

Phase Motion at $n_2 \neq 0$

In this case the coordinates of fixed points are:

$$x_1 = 0, \quad u_1 = 0; \quad x_{2,3} = 0,$$

$$u_{2,3} = [-K_2^2 \pm (K_2^2 - 48I^2 \Delta n n_2)^{1/2}]/6In_2. \quad (15)$$

As system (6) is invariant to coordinate rotation at $\pm 120°$, we can obtain four other fixed points:

$$x_{4,6} = \pm u_2\sqrt{3}/2, \quad u_{4,6} = -u_2/2;$$

$$x_{5,7} = \frac{\pm u_3\sqrt{3}}{2}, \quad u_{5,7} = -\frac{u_3}{2}. \quad (16)$$

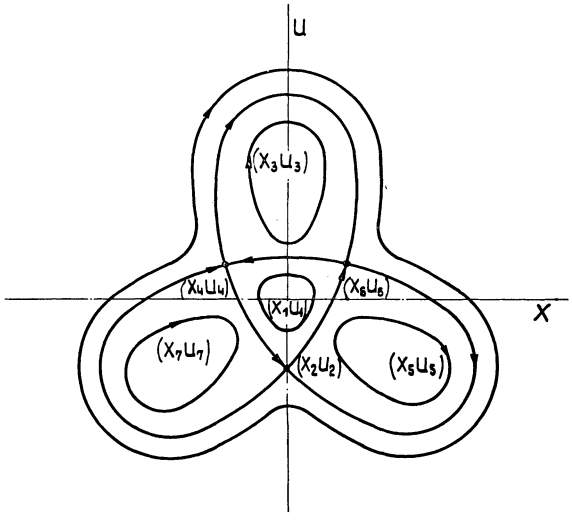

FIGURE 3 Phase space plot for $\Delta n > 0$ and $n_2 < 0$.

Figure 3 shows the character of phase trajectories for $K_2 > 0$, $\Delta n > 0$ and $n_2 < 0$. (x_2, u_2), (x_4, u_4) and (x_6, u_6) are unstable fixed points defining the stable region where representative points move around the centre point (x_1, u_1). Outside this region representative points do not go to infinity but move around the centre fixed points (x_3, u_3), (x_5, u_5) and (x_7, u_7). In order to have the required picture at the septum magnet entrance, the following condition should be fulfilled:

$$|u_3|\sqrt{3}/2 > x_s$$

or taking into account (15)

$$|n_2| < |K_2|/2x_s\sqrt{3}. \quad (17)$$

The numerical estimate gives: $|n_2| < 3 \cdot 10^{-5}$ cm^{-2}.

From the expression

$$\frac{\partial u_2}{\partial \Delta n} = 4I(K_2^2 - 48I^2 \Delta n n_2)^{-1/2} \quad (18)$$

one can see the influence of n_2 on the change rate of the stable region. In our case (Figure 2, curve n_r) for -10 cm $< x <$ 10 cm $n_2 < 0$. It reduces $|\partial u_2/(\partial \Delta n)|$ for $\Delta n > 0$ and increases for $\Delta n < 0$.

Momenta Spread Influence

Taking into account the momentum spread, the term

$$K_{0p} = K_2 \frac{1 - n + \Delta p/p_0}{1 - n - n\Delta p/p_0} \left(\frac{R_c \Delta p/p_0}{1 - n} \right)^2 \quad (19)$$

appears in Eq. (5). The form of this term is similar to that of the term with a dipole component and its influence is similar as well. The shift of the effective value n is equal to

$$\delta n = -\frac{K_{0p} K_{2p}}{[4 - (1-n)I]I}, \quad (20$$

where

$$K_{2p} = K_2(1 - n + \Delta p/p_0)/(1 - n - n\Delta p/p_0).$$

In this case the fixed point coordinates are:

$$x_{1p} = 0, \quad u_{1p} = \frac{3K_{0p}}{4 - (1-n)I};$$

$$x_{2p} = 0, \quad u_{2p} = -\frac{4\Delta nI}{K_{2p}} + \frac{3K_{0p}}{4 - (1-n)I};$$

$$x_{3p,4p} = \pm 2\sqrt{3}\frac{\Delta nI}{K_{2p}},$$

$$u_{3p,4p} = \frac{2\Delta nI}{K_{2p}} + \frac{3K_{0p}}{4 - (1-n)I}.$$

The instantaneous angle spread at the *FM* entrance is $u = u_{3p} - u_3$. The numerical estimate gives $\Delta\alpha = \pm 0.003$ mrad for $\Delta p/p_0 = \pm 2 \cdot 10^{-4}$. Under these conditions the amplitude gain changes by ± 10 per cent.

3. COMPUTATION OF PARTICLE MOTION UNDER RESONANCE CONDITIONS

The parameters of the extraction system obtained above were used as initial data for a computer.

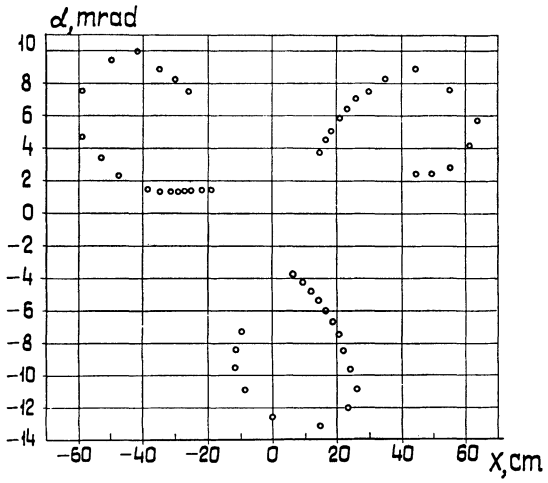

FIGURE 4 Phase coordinates of particles in successive turns showing an arrested growth of amplitudes at large radii caused by a limited expansion of the perturbation $\Delta B_z(x)$.

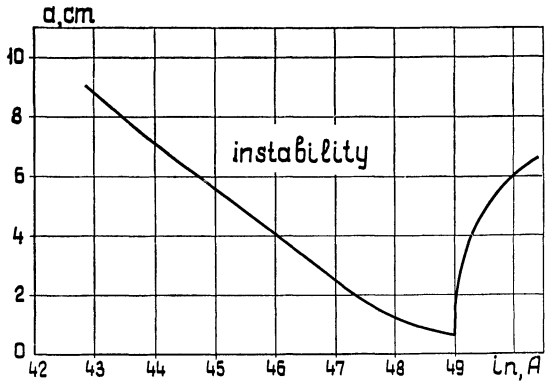

FIGURE 5 Stable area versus winding $P1$ current. Winding $P2$ currents: $i(R_0 \pm 40) = 148$ A, $i(R_0 \pm 20) = 62$ A.

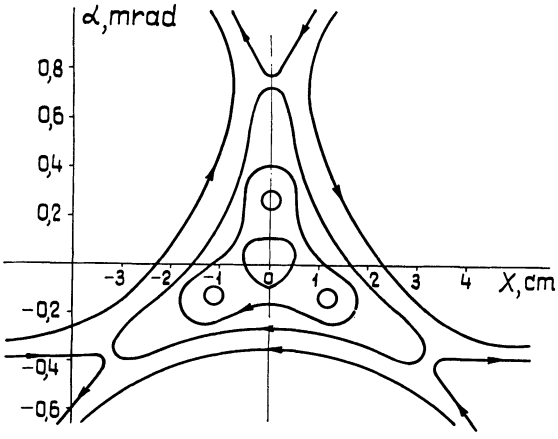

FIGURE 6 Stabilization of the small amplitude growth caused by nonuniformity of the $n_r(x)$ distribution.

The computation of the particle trajectories taking into account the measured $n(x)$ (Figure 2), the influence of pole-face conductors and accelerator structure was made by means of the FORTRAN program MFIELD[9] that calculates multiturn particle motion and the field inductance $B_0 = 10$ kG. The analysis of the curve shape $\Delta B_z(x)$ (Figure 2) shows that the sextupolar dependence is fulfilled more exactly if the current relation i_{2A}/i_{2B} in the winding conductors $P2$ equals 0.42. Representation of $\Delta B_z(x)$ as a power series in x shows that from $x = \pm 40$ cm the contribution of high order terms increases ($b_4 x^4$, $b_6 x^6$ and so on). This causes the appearance of stable regions (Figure 4) and limits the choice of the maximum values x_s and Δx_s being equal in this case to 35 and 17 cm, respectively. The computed currents of $P2$ are $i(R_0 \pm 40) = 148$ A and $i(R_0 \pm 20) = 62$ A. Figure 5 shows the dependence of the stable amplitude boundary on the current $P1$ for the indicated currents in the $P2$ winding. The stable region is minimum if $i_n = 49$ A. From Figure 2 (curve n_r) one can see that this curve may be presented near R_0 in the form: $= n_r n_0 + n_2 x^2 + \ldots$; $n_2 = 1.5 \times 10^{-4}$ if $i_n = 49$ A. This value n_2 is significantly larger than the limit value obtained from (17). This leads to the appearance of stable 'islands' in the R_0 vicinity (Figure 6), therefore the particles with $a < 0.6$ will not be extracted. As follows from Ref. 18, the asymmetry of the stable region relatively at $i_n = 49$ A ($\Delta n = 0$) is explained by the influence of n_2 (Figure 5) as well. A more uniform distribution of $n_r(x)$ may be created by means of an additional conductor placed at R_0.

Figure 7 presents the phase space plots at the *FM*

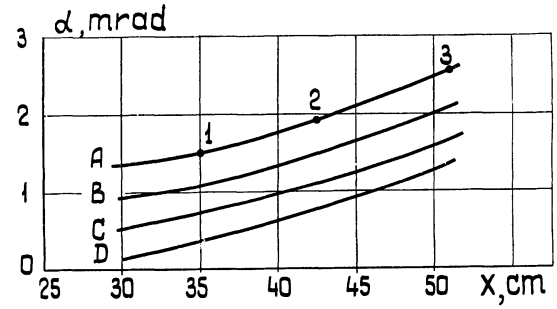

FIGURE 7 Phase space plots at the *FM* entrance for different currents in the winding P1: curve *A*. $i_n = 42.84$ A (extraction beginning); curve *B*. $i_n = 45.1$ A; curve *C*. $i_n = 47.32$ A; curve *D*. $i_n = 49$ A (extraction end).

entrance during the extraction for different currents in the $P1$ winding (curves A, B, C, D). The average angle of particles at $x_s = 35$ cm decreases from 1.55 mrad at the beginning of the extraction up to 0.35 mrad at the end.

The maximum rate di_n/dt of the current change in the $P1$ winding and, consequently, a minimum extraction time are defined under the following condition: the time when the particle with a small amplitude is in the unstable region must be more than that required for the particle amplitude blowup. The computations showed that the value $di_n/dt = 10$ A/msec ($\tau = 1$ msec) was sufficient for the extraction of the particles with an initial amplitude 1 cm. For an extraction time of 1000 msec minimum initial amplitudes of the extracted particles are now defined by the value of n_2.

4. COMPUTATION OF THE TRANSPORT SYSTEM

The task of computing the internal transport system was

(a) to define the first stage parameters giving a minimum distortion of the transverse beam phase space when particles pass through the second quadrant fringing field and to obtain the beam sizes at the second stage entrance determined by its aperture;

(b) to compute the field and gradient values of the second stage that allows to preserve an effective beam emittance in the third quadrant fringing field and to transport the beam out of the quadrant by means of the external transport system. This computation was made by the FORTRAN program FORM[1] for an accelerator guide field of 10 kG with its distribution obtained from magnetic measurements.

The phase coordinates of 3 points that characterize the edges and the centre of the beam at the *FM* entrance at the extraction beginning (Figure 7; curve A; points 1, 2, 3) were taken as initial conditions in a horizontal plane to compute the first stage. In order to compute a vertical motion for each of these points, a set of initial conditions in the $(z-z')$ plane, corresponding to the circulating beam emittance ($a_z = 2$ cm), was taken.

The value of the septum magnet field B_F and the gradient G_F were computed by means of iterations for so-called 'under-focusing' ($d\Delta x/dG_F(< 0)$ and 'superfocusing' ($d\Delta x/(dG_F) < 0$) conditions where Δx is a horizontal beam size at the second stage entrance. Figure 8 shows the radial particle

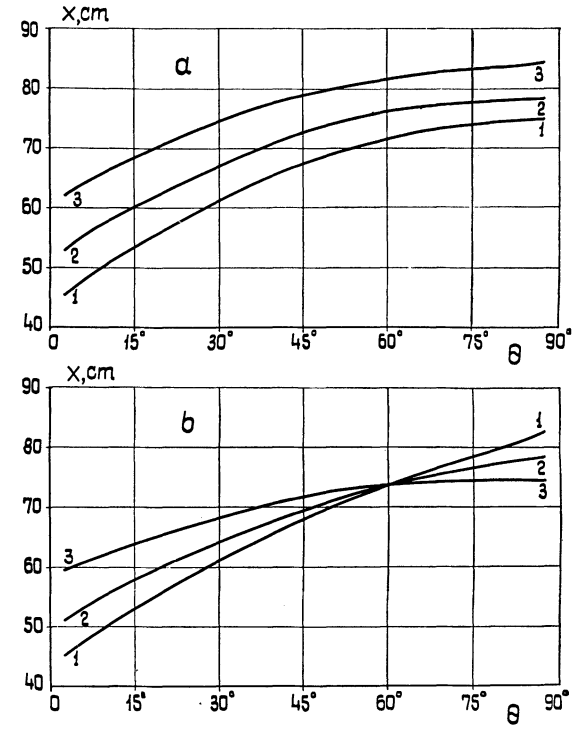

FIGURE 8 Particle trajectories in the second quadrant for underfocusing (a) and superfocusing (b) conditions. Curves 1, 2 and 3 refer to inside, central and outside particles at the *FM* entrance respectively. Along the axis θ, the azimuth in degrees, is plotted.

trajectories in the quadrant II for 'under-focusing' (a) and 'superfocusing' (b) conditions. As different trajectories for the first condition pass the regions with a distinct field index n, the radial phase at the second stage entrance is strongly distorted (Figure 9, curve a). Due to this reason, the vertical phase ellipses are oriented differently and the effective vertical emittance sufficiently increases (Figure 10 (a)). The field index correction by means of additional pole-face conductors requires an amount of current about 30 kA and is quite impossible. The use of a sextupole lens in the first stage decreases the horizontal phase nonlinearity, but the vertical phase ellipses are oriented in different ways.

The superfocusing condition is preferable though in this case the values of B_F are 1.1 times and G_F −2

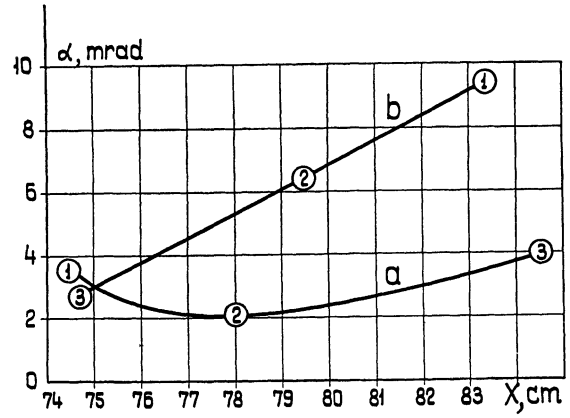

FIGURE 9 Radial phase space plots at the *BM* entrance for underfocusing (curve *a*) and superfocusing (curve *b*) conditions. Numbers 1, 2 and 3 represent the same as in Fig. 8.

times more than for the underfocusing condition The main property of this condition is that the trajectories 1 and 3 are crossed over some azimuth, and the average field index along each of them is approximately equal. Figure 9 (curve *b*) and Figure 10(b) show the phase space plots under these conditions in horizontal and vertical planes, correspondingly. For these conditions $B_F = 1660$ G (the magnet length is 1.7 m) and $G_F = 99.4$ G/cm (the lens length is 1 m).

The beam angle change at the *FM* entrance during the extraction time (Figure 7) is compensated by changing the *FM* field so that the beam position at the second stage entrance is constant.

The extraction magnet of the second internal stage permits bending a beam with maximum energy at an angle of about 0.08–0.09 mrad. In connection with the reconstruction of the magnet yoke of the synchrophasotron this value was made more precise. This angle was 0.08398 rad relative to the straight section axis (Figure 1). The beam size at the accelerator exit is defined by the aperture of the external quadrupole lenses (16–20 cm).

The main stage of the external transport system focuses the extracted beam onto the target of the south experimental hall. Figure 11 gives the horizontal and vertical phase space plots at the external target placed at the distance $T = 1.5$ m from the exit of the last quadrupole lens. The horizontal beam size is about 0.55 cm, divergence being 18 mrad; the vertical beam size is 0.29 cm and divergence being 0.64 mrad.

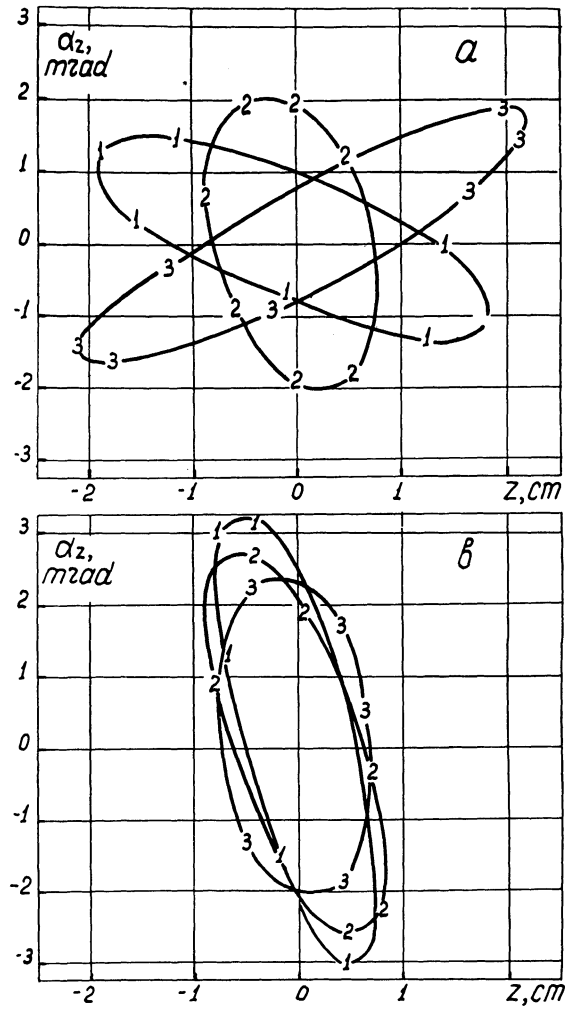

FIGURE 10 Vertical phase space plots at the *BM* entrance for underfocusing (a) and superfocusing (b) conditions. Numbers 1, 2 and 3 represent the same as in Fig. 8.

One can expect some possible change of the computed and experimental beam parameters due to simplification of the accelerator field description and obtaining the beam parameters at the *FM* entrance under stationary resonant conditions. The influence of these factors may be compensated by fine adjustment of the extraction system.

5. STABILIZATION OF THE EXTRACTED BEAM

The range of the radial betatron oscillations of the particles in the stable region is a function of current $a = a(i_n)$. This function means that at a given

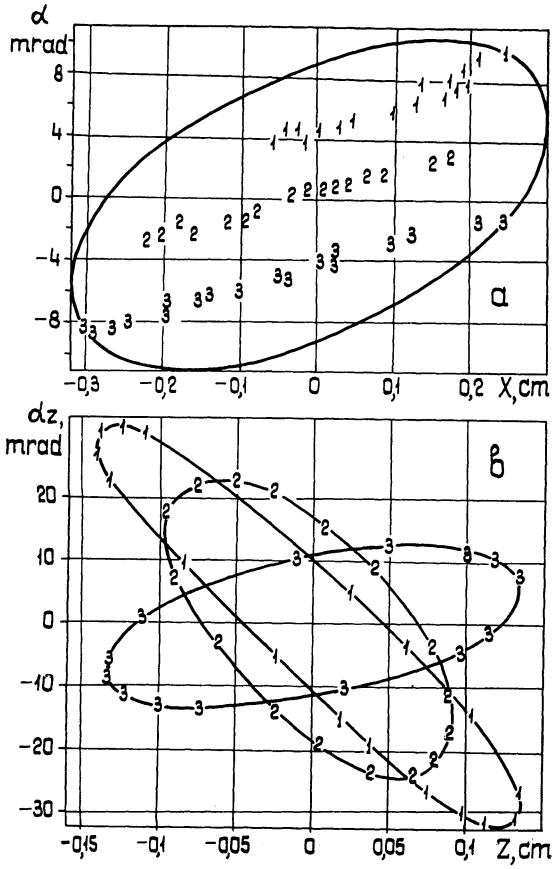

FIGURE 11 Horizontal (a) and vertical (b) phase space plots in the first external target. Numbers 1, 2 and 3 represent the same as in Fig. 8.

current i_n all particles with amplitudes from 0 up to $a(i_n)$ are stable. The amplitude distribution of particles in the circulating beam is described by a function $f(a)$ similar to the Rayleigh distribution.

In order to maintain the beam current

$$j(t) = -I_0 f(a) \frac{da(i_n)}{di_n} \frac{di_n}{dt} \tag{21}$$

(I_0 is the number of particles in the circulating beam) constant during the extraction, an analog feedback is introduced into the circuit supplying the winding $P1$ (Figure 12).

A value proportional to the intensity I_0 measured by means of a monitor (pickup electrodes) directly before ejection is used as a reference potential. This gives homogeneous extraction current during the extraction time independent of the accelerated beam intensity. The voltage δI_0 (δ is the transverse coefficient of $Q1$) is fixed by the analog memory consisting of switches $W1$, $W2$, a capacitor C and an amplifier $Y1$ with high input impedance ($R_i = 40$ MΩ). The regulation of the reference voltage $U_0 = K\delta I_0$ is realized by a potentiometer $R1$. The voltage $U = \beta j(t)$ is generated by a beam current monitor $Q2$. In order to exclude the in phase noise arising in a comparatively long communication line (about 400 m), a differential amplifier generating a correction signal $\Delta U =$

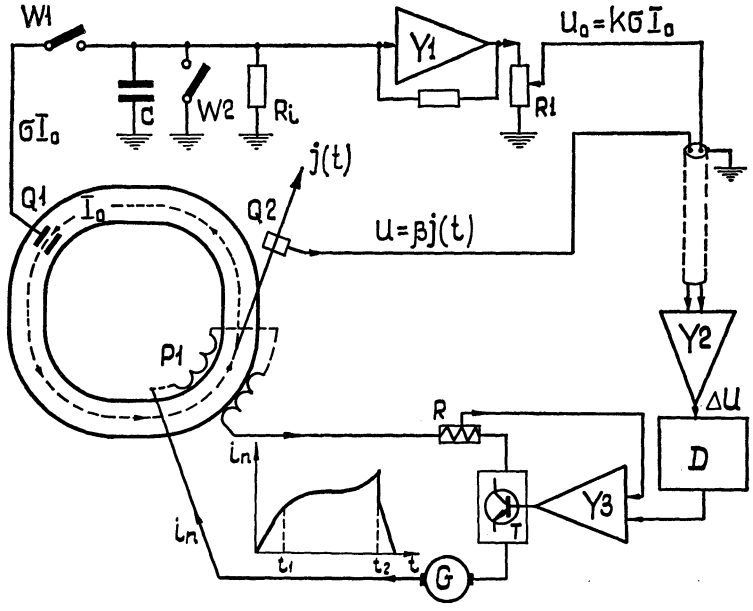

FIGURE 12 Block diagram of the extracted beam current feedback.

$U-U_0$ is placed in immediate proximity to the operating devices; also the communication line is two-wire.

According to (21), the adjustment of the extracted beam current may be realized by varying the rate of i_n. The correction signal ΔU from the output of the differential amplifier $Y2$ is fed into the unit D. The output voltage of the unit D

$$U_D = U_b + q\frac{n_b - n_r}{\tau}\, t - \gamma \int_0^t \Delta U \mathrm{d}t \qquad (22)$$

(U_b is the voltage corresponding to the $P1$ winding current at which the extraction begins; q and γ are the coefficients of proportionality) is compared with that of the resistor R proportional to the $P1$ winding operating current by means of the differential amplifier $Y3$. The result of comparison is fed into the transistor regulator T correcting the current i_n during the spill time $(t_1 - t_2)$.

A slow decrease of the beam average angle at the first stage entrance during the extraction is compensated by varying the *FM* magnetic field with the help of feedback that allows keeping the beam average angle constant at the first stage exit and, therefore, its space position at the *BM* entrance.

6. MAGNETS AND LENSES

The length of the magnet *FM* [10] with a gap aperture 65×220 mm^2 is 1.7 m. The septum thickness is 2 mm. The upper magnitude of the magnetic field is 2.5 kG. The field inhomogeneity lies within ± 0.2 per cent.

The one meter long quadrupole lens is a 'semi-lens' with a square aperture. It has a neutral pole made of a 0.35 mm thick steel plate that represents a magnetic septum.

The aperture of the 3 m long magnet *BM* is 65×190 mm^2. The thickness of its septum is 25 mm. The magnetic field is 13 kG. In the working part of the gap (about 90 per cent of its transverse size) the magnetic field inhomogeneity is within ± 0.2 per cent.

The Panofsky lens *BL* is 0.7 m in length. Its aperture is 65×216 mm^2.

7. EXPERIMENTAL RESULTS

The experiments have been carried out at 8, 10 and 12 kG of the accelerator main field. As the results obtained for these fields are similar, the data cited below correspond to $B_0 = 10$ kG.

The resonance development proved to be sensitive to the current relation in the branches $P2$–A and $P2$–B. Its optimum value is found to be 0.42. The winding branches are supplied by one power generator to keep this relation constant. The 'jump' tuning is realized by adjusting $P2$ winding current. The beam is observed with the help of a scintillation screen placed at the *FM* entrance and TV camera. The latter allows estimation of the horizontal beam size with an accuracy of about 0.5 cm. The nominal 'jump' of 17 cm has been obtained at a total current of 212 A in the $P2$ winding (the calculated value is 210 A). The beam photograph at the *FM* exit is shown in Figure 13 where the dark strip is the septum projection. The photograph was made when the *FM* current was off. This made it possible to estimate the effective thickness of the septum; it proved to be about 5 mm. The effective thickness increase by 3 mm is mainly determined by septum manufacture inaccuracies and magnet installation errors.

The resonance begins at a $P1$ winding current $i_n = 40$ A. The extraction comes to an end when $i_n = 50$ A. As the field index depends on the accelerator operating region (Figure 2), the current i_n corresponding to the extraction beginning proved to be critical to the beam radial position. It is found that a change of the beam centre by ± 4 cm relative to R_0 requires an i_n change of ± 5 A. The system that allows establishing the beam centre position at the extraction beginning with an accuracy of ± 0.2 cm was used to reduce radial shifts.

The oscillograms in Figure 14 illustrate the effect of the extracted beam current feedback. The spill time is about 400 msec. The modulation observed is caused by current ripples in the $P1$ winding. Methods of suppressing this modulation are under development now.

The *FM* current varies from 10.7 kA (2060 G) at the extraction beginning up to 11.4 kA (2200 G) at the end. This corresponds to a beam angle variation at the *FM* entrance by about 0.9 mrad. The increase

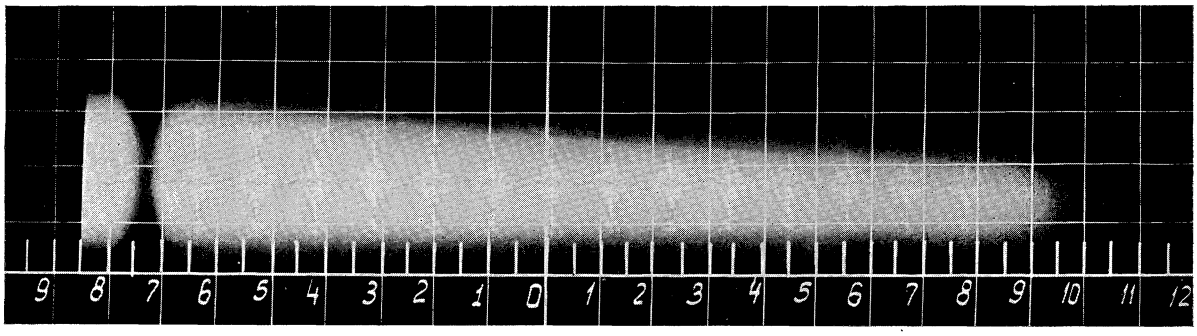

FIGURE 13 · Beam at the magnet *FM* exit. Scales—in cm.

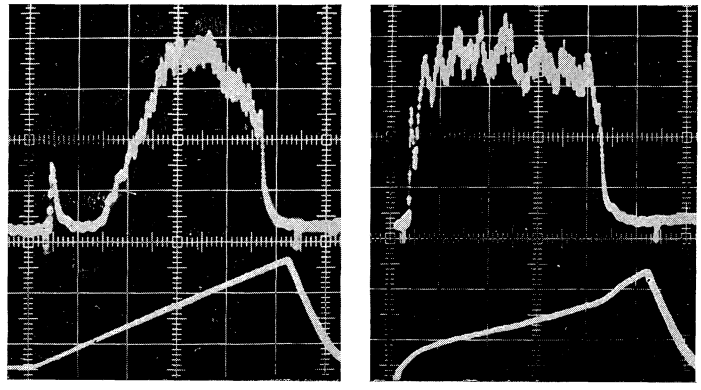

FIGURE 14 Current of the extracted beam (upper ray) and current i_n (lower ray). (a) linear law without feedback; (b) with feedback. Time scale: 0.1 sec per division.

of the field magnitude in comparison with the calculated one ($\approx$20 per cent) can be explained by existing distortions of the accelerator magnetic field.

Removal of the distortions of the beam phase space caused by edge field nonlinearities is realized by adjustment of the first stage operating conditions that permit obtaining a horizontal intermediate image in the second quadrant. Figure 15 shows a photograph of the beam obtained in underfocusing conditions (lens gradient $G_F = 86$ G/cm) at the entrance of the magnet *BM*. The asymmetrical form of the beam is due to various orientation of the vertical phase ellipses for the internal and external trajectories as was predicted by computations. The photograph in Figure 16 illustrates the compensation of this effect in superfocusing conditions ($G_F = 102$ G/cm). The photograph of the beam on the external target is shown in Figure 17. The linear magnification of the second lens doublet is equal to 0.122 for the horizontal plane and 0.0877 for the vertical plane. Emittance measurements gave 95π mm mrad (horizontal plane) and 50π mm mrad (vertical plane) which exceeded the calculated values by 3 and 1.3 times, respectively. The difference observed is due to beam jitters caused by ripples in the *FM* power supply. A rapid feedback

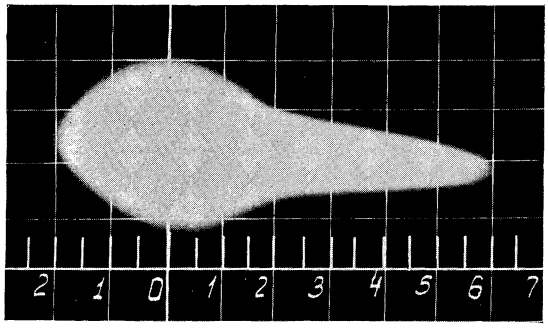

FIGURE 15 Beam at the magnet *BM* entrance (underfocusing condition). Scales—in cm.

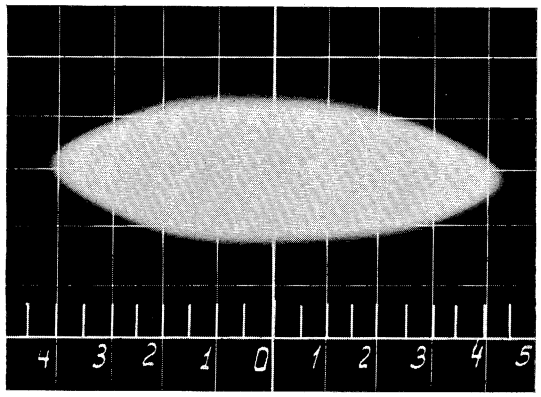

FIGURE 16 Beam at the magnet *BM* entrance (super-focusing condition). Scales—in cm.

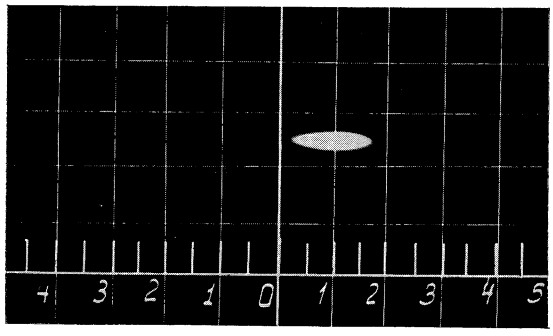

FIGURE 17 Beam at the external target. Scales—in cm.

using a regulator in the *FM* power circuit will minimize these effects.

Extraction losses depend mainly on the passage of particles through the *FM* septum since large enough apertures exclude losses due to drifts and instability of the parameters of extraction elements. Some additional contributions to the beam losses are caused by passing the beam through the indication δ-ray plates mounted at the entrance of the magnet *BM*. Primary measurements of the efficiency were made using the reaction C_{12} (p, pn) C_{11}. The results showed that the efficiency of the extraction system was not less than 90 per cent. More accurate measurements were carried out by detecting secondary particle fluxes proportional to the number of protons remaining in the accelerator. According to the fluxes in conditions with extraction and without it, the efficiency was found to be equal to (94 ± 0.5) per cent.

At present, besides protons, the extraction of deuterons and α-particles has been performed as well.

ACKNOWLEDGEMENTS

In conclusion the authors would like to express their gratitude to Professor A. M. Baldin and Dr. I. N. Semenyushkin for their permanent interest and support of this work. The authors are deeply grateful to their colleagues V. N. Buldakovsky, V. P. Zabolotin, A. I. Kryukov, Yu.F. Kusagin, V. S. Mironov, O. N. Tsyslyak, V. I. Chernikov who took part in the creation and adjustment of the system. We also express our appreciation to Drs. S. A. Averichev, I. A. Eliseeva, L. A. Leonov, V. P. Matveeva, E. A. Matyushevsky and A. A. Smirnov for their participation in different stages of the work. The authors are grateful to A. P. Tsarenkov for the possibility of using the apparatus necessary for maintaining the beam with a high accuracy at the given radius. We take an opportunity to express our acknowledgement to Professor M. Conte for his collaboration during analytical calculations.

REFERENCES

1. B. V. Vasilishin, I. B. Issinsky, E. M. Kulakova and V. A. Mikhailov, Report JINR, BI-9-6536, Dubna, 1972.
2. A. A. Averichev *et al.*, Report JINR, B2-9-6896, Dubna, 1973.
3. M. R. Harold, Report RHEL/RI 73, 1968.
4. L. N. Belyaev, A. A. Smirnov, N. I. Pavlov, Report JINR, 9-4358, Dubna, 1969.
5. M. Conte, Report JINR, E-9-4925, Dubna, 1970.
6. M. Conte, *Nucl. Instr. & Meth.*, **62**, 269 (1968).
7. N. N. Bogolyubov, Yu. A. Mitropolsky, *Asymptotic Methods in the Nonlinear Oscillation Theory* (Moscow, 1958).
8. A. Maschke and K. Symon, *Proc. of All-Union Conf. on Charged Part. Accelerators*, Vol. I, p. 516 (Moscow, 1970).
9. B. V. Vasilishin and E. M. Kulakova, Report JINR, 9-6720, Dubna, 1972.
10. L. P. Zinoviev, I. B. Issinsky, V. S. Mironov, S. A. Novikov, V. I. Chernikov, Report JINR, 9-6537, Dubna, 1972.

Received 18 July 1973